

Spin Torque Efficiency and Analytic Error Rate Estimates of Skyrmion Racetrack Memory

D. Suess¹, C. Vogler², F. Bruckner¹, C. Abert²

¹Doppler Laboratory, Institute of Solid State Physics, Vienna University of Technology, 1040 Vienna.

²Institute of Solid State Physics, Vienna University of Technology, 1040 Vienna.

Abstract: In this paper the critical currents as well as the thermal stability of skyrmion racetrack like structures is investigated. It is reported that the pinning sites which are required in order to allow for thermally stable bits significantly increases the critical current densities to about $j_{\text{crit}} = 0.62 \text{ TA/m}^2$ to move the bits in skyrmion like structures. By calculating the thermal stability as well as the critical current we can derive the spin torque efficiency which is $\eta = \Delta E/I_c = 0.19 k_B T_{300}/\mu\text{A}$ which is in similar range of simulated spin torque efficiency of MRAM structures. Finally it is shown that the stochastic depinning process of any racetrack like device require very narrow switching or depinning time distribution in order to avoid thermally written in errors or special current profiles allowing for a clock cycle.

1. Introduction

Magnetic skyrmions are topological spin structures which can exist in materials at zero external field due to non-centrosymmetric lattice or in magnetic ultrathin films with broken inversion symmetry^{1,2}. In various studies skyrmions are suggested as a future data storage device due to the small electrical currents to move these topological structures²⁻⁸. An important property for any storage device is the long time thermal stability of the stored information. Since the presence and the absence of a skyrmion represents bit “1” and bit “0” the stability between these two states is the essential feature for the long time stability. These two states have to be separated by an energy barrier which can be realized by a pinning center. In the presenting work the pinning centers are realized by constrictions in the wire with the Dzyaloshinskii-Moriya interaction (DMI) which allows the formation of skyrmions.

2. Model

In order to study the creation and motion of skyrmions a spin drift diffusion model is used as described by Zhang et al.⁹. The discretization of the continuum model is done using a hybrid finite

element / boundary element method as presented in detail in Ref^[10]. In the used model beside the magnetization as function of time, the spin accumulation s and the electrical potential u are calculated as function of input currents. The total energy of the magnetic system is composed of the exchange energy, the magnetostatic energy, the anisotropy energy and the Zeeman energy¹¹. In order to take into account for the interface DMI the additional energy contribution is added to the effective field¹²,

$$E_{DMI} = \int D [m_n (\nabla \cdot \mathbf{m}) - \mathbf{m} \cdot (\nabla m_n)] dV \quad (1)$$

where the coupling constant D and the projected magnetization m_n is define by $m_n = \mathbf{m} \cdot \mathbf{n}$ and \mathbf{n} is the normal vector of the interface. The effective field is the negative functional derivative of the total energy with respect to the magnetic polarization \mathbf{J} , leading for the DMI contribution to

$$\mathbf{H}_{DMI} = -\frac{\delta E_{DMI}}{\delta \mathbf{J}} = -\frac{2D}{J_s} [\mathbf{n} (\nabla \cdot \mathbf{m}) - \nabla (\mathbf{n} \cdot \mathbf{m})] \quad (2)$$

3. Results

3.1 Critical current densities

In the following the magnetization and spin accumulation is investigated as function of time for the current driven motion of a skyrmion for the geometry as shown in Fig. 1. The structure consists of three leads. The pinned lead is next to a pinned layer with fixed magnetization in order to generate a skyrmion via spin transfer torque via the spacer layer. Two leads at the very end (front lead, and back lead) are used to drive the created skyrmion. The front and back lead has the dimensions of 30 nm x 90 nm x 3nm, respectively. The dimensions of the DMI wire are $l = 600$ nm, $w = 90$ nm, $t = 1.8$ nm if not state differently. The diameter of the notches as well as the spacer (thickness $t = 1.5$ nm), pinned layer (thickness $t = 9.0$ nm) and pinned lead (thickness $t = 6.0$) is $d = 60$ nm. The magnetic and electrical material parameters of the wire are: anisotropy constant $K_1 = 0.6$ MJ/m³, with the easy axis perpendicular to the film (z-axis), saturation polarization $J_s = 0.72$ T, exchange constant $A = 15$ pJ/m, $\alpha = 0.02$, the exchange strength between the conducting electrons and magnetization $J = 4.1 \times 10^{-20}$ J, the dimensionless polarization parameters $\beta = 0.9$, $\beta' = 0.8$, the spin flip relaxation time $\tau_{sf} = 5 \times 10^{-14}$ s, the diffusion constant $D_0 = 10^{-3}$ m²/s and the DMI constant is $D = 3 \times 10^{-3}$ J/m².

The pinned layer which is used to inject a skyrmion has an anisotropy constant of $K_1 = 0.6$ MJ/m³ and the magnetization is antiparallel to the initial magnetization in the DMI wire. In order to nucleate a skyrmion a current is applied between the pinned lead and the back lead. A skyrmion is nucleated for a current density of 50 GA/inch². The nucleated skyrmion has magnetization parallel to the pinned

layer which leads to pinning of the skyrmion due to the strayfield of the pinned layer. In the following a current pulse is applied in order to move the skyrmion into the center of the DMI wire. At this position no significant strayfield due to the pinned layer is acting on the skyrmion and the critical currents in order to move the skyrmion over the pinned sites can be studied accurately.

In *Fig. 2* the critical current in order to move the skyrmion over the pinning sites is studied. Two different geometrical realization of the pinning sites are investigated. The diameter of the pinning sites is $d = 60$ nm (left) and $d = 120$ nm (right), respectively. The current density rise time is $r = 11$ GA/(m²ns), where the current density is measured in the DMI wire between two notches. The current density is applied at the back lead and the potential is fixed to zero at the front lead. The left column in *Fig. 2* shows simulation where a positive current is applied at the back lead. Here, the skyrmion moves to the left. Interestingly, the critical current density to overcome the pinning site is smaller for the narrow pinning site ($j_{\text{crit}}=0.62$ TA/m² for $d = 60$ nm) compared to the pinning site with $d = 120$ nm ($j_{\text{crit}}=0.67$ TA/m²). This effect is unexpected since the pinning field of a domain wall that is driven by an external field is proportional to the derivative of the cross section area with respect to the moving direction of the domain wall ($H_p \propto \partial A / \partial x$ as given by Eq.

Fehler! Verweisquelle konnte nicht gefunden werden. in the Appendix). This analytical obtained dependence of domain walls is qualitatively in agreement with results of micromagnetic simulations of pinning fields of Ref. ¹³. Similar results are also reported for critical depinning currents obtained from experiments and simulations Ref. [¹⁴]. The origin of large pinning currents for the larger diameter of the pinning sites in the case of skyrmions is an interesting study for future work.

In contrast to the previous simulations in the following we present skyrmion dynamics when current pulses are applied. Starting from an equilibrium configuration of the skyrmion in the center between two pinning sites the current is increased from zero to j_{max} within 1 ns. This current is kept constant for the next 10 ns. In *Fig. 3* an interesting phenomena is shown which will show a significant challenge for skyrmion storage devices. If $j_{\text{max}} < 0.27$ TA/m² as shown in the two top images of *Fig. 3* the current is too small to overcome the pinning sites. For an intermediate current density of $j_{\text{max}} = 0.55$ TA/m² the problem of annihilation of the skyrmion can be observed. This shows that the discussed topological protection ^{8,15} does not prevent skyrmions from annihilation in finite size systems. On the other side a full topological protection which theoretically also rules out a transformation from a homogenous state into a skyrmion state would also be disadvantage for applications since it would rule out the possibility to create a skyrmion in a deterministic way. Interestingly if the current density is further increased to $j_{\text{max}} = 0.82$ TA/m² the skyrmion is no longer annihilated and it is possible to overcome the pinning site. This shows that properly designed current strength are required in order to move skyrmions in magnetic structures with pinning sites.

The used model which couples the magnetization dynamics with the spin accumulation self – consistently solves beside the magnetization as function of time also for the electrical potential as function of time as well as the spin accumulations \mathbf{s} . The spin accumulation which depends on the magnetization in turn acts via the exchange strength between the conducting electrons and magnetization J as a torque term on the magnetization. The three components of the spin accumulation are shown in *Fig. 4* for a current strength just before switching over the pinning center as shown by the position of the skyrmion at bottom of *Fig. 4*. It is important to note that all three components of the spin accumulation are unequal zero and in the same order of magnitude. This is in contrast to the simplified but often used model of Zhang and Li¹⁶. In contrast to the Zhang and Li model which preserves the magnitude of the magnetization this is not the case in the also popular model of Thiaville et al.¹⁷. However if the magnetization in the model of Thiaville et al. is constrained to be conserved the model is equivalent to the Zhang and Li model. The used coupled spin drift diffusion model is equivalent to the model of Zhang and Li for the limiting case of a vanishing diffusion constant, $D_0 = 0$. The advantage of the Zhang and Li model compared to the coupled magnetization and spin drift diffusion is the simplified calculation of the spin transfer torque, which can be expressed explicitly as function of the magnetization. However, the question has to be asked if the approximation leads to different results and the combined solution of the magnetization and spin accumulation is required for accurate results.

Hence, we studied in the following the critical current densities in the limit of $D_0 = 0$ as shown in *Fig. 5* and compare it to the fully coupled model. It is important to note that only the x-component of the spin accumulation is not zero in the limit for $D_0 = 0$. Even more important is the fact the simplified model for $D_0=0$ predicts a critical current of $j_{\text{crit}}=1.05 \text{ TA/m}^2$ which is by about a factor 1.7 higher than the predicated critical current $j_{\text{crit}}=0.62 \text{ TA/m}^2$ within the full model. Hence, the additional computational effort of the full model which requires the self-consistent solution of the spin accumulation and magnetization is essential to obtain accurate results. Another effect which is more pronounced in the limiting case of $D_0 = 0$ compared to the full model including $D_0 > 0$ are breathing modes as shown in *Fig. 5*. Here, the skyrmion precesses on an elliptical orbit as well as changes its size periodically for critical current as function of time. Here a current density is applied which is slightly smaller than the critical current density to overcome the pinning site. A similar effect was found in dynamically stabilized skyrmion, which exists even when dipolar interactions and DMI are absent¹⁸.

3.1 Thermal stability and spin torque efficiency

As mentioned in the introduction a must for any potential storage application is the thermal stability of the stored information. The average lifetime τ of magnetic states can be expressed within the framework of the transition state theory as,

$$\tau = \frac{1}{f_0} \exp\left(\frac{-\Delta E}{k_B T}\right) \quad (3)$$

where, ΔE is the energy barrier between two stable states and f_0 is the attempt frequency which is in the range of 1 to 100 GHz and depend on the anisotropy field and various other magnetic properties as well as temperature^{19,20}. In order to obtain thermally stable bits in hard disk recording an energy barrier of about $\Delta E \geq 50k_B T_{300}$ is a common requirement. In the following we present simulations of the energy barrier using the string method taking into account for all energy terms including the DMI interaction²¹. The two stable magnetic states which are required as an input for the string method are the states between the pinning sites as shown in *Fig. 6* by the image indexed with $i=0$ (initial state 1) and the image indexed with $i = 19$ (initial state 2). On the right column of *Fig. 6* the simulation correspond to a simulation with $l = 500$ nm, $w = 75$ nm, $t = 1.5$ nm and $d = 50$ nm. The images indexed between $i = 2$ and $i = 18$ show magnetic states along the minimum energy path (MEP). This path is the most probable path which is triggered by thermal fluctuation if no external field or current is applied. The energy along this MEP is shown in *Fig. 7* (black line) as function of path index i . The reason why the stable state $i = 0$ as lower energy as the state with $i = 19$ is due to the strayfield of the pinned layer which is magnetized in the direction of the skyrmion and stabilizes the skyrmion. The smaller energy barrier of these two is $\Delta E = 16.4 k_B T_{300}$ which does not provide sufficient thermal stability.

One way in order to increase the energy barrier of the device but not increasing the critical current densities to overcome the pinning site is to increase the film thickness. Depending on the origin of the DMI interaction the DMI is an interface effect or a bulk effect. In the case of an interface effect the effective DMI constant scales with one over the film thickness and increasing the film thickness in turn would require to reduce the DMI constant which was not done in the simulations. However, multilayer structures such as multiple repetitions of asymmetric Pt/Co/Ir multilayer may allow to increase the film thickness and keeping an high effective DMI constant²². As it can be seen in *Fig. 8* the energy barrier approximately linearly increases as function of the film thickness. The simulations indicate that film thicknesses larger about $t > 3.8$ nm are required in order to obtain structures with $\Delta E > 50.0 k_B T_{300}$, where the skyrmions are sufficiently pinned so that they can be expected to be thermally stable.

In the next step we aim to answer the question how the energy barrier depends on the structure size. Hence, in the following all spatial coordinates are scaled by a factor *scale size* = 0.9. For this situation the MEP is shown in *Fig. 6* (left column). It can be seen that the skyrmion is annihilated and nucleated again along the MEP. This strongly suggest that also for current driven skyrmions a critical size exists which has to be exceeded in order to avoid annihilation of the skyrmions. As shown in *Fig. 3* for current driven skyrmions it is not possible to define one critical size above which the skyrmions are stable. The critical size depends on various parameters such as the applied current strength and current rise time. However simulations show that the critical size for stable skyrmion motion for is similar as obtained from the MEP simulations of *Fig. 6*. The energy along the MEP for the reduced size is shown in *Fig. 7* (red dashed line) . It can be seen that due to the annihilation of the skyrmion and nucleation the energy barrier is significantly reduced, which alone makes this size unattractive for a storage device.

The energy barrier as function of the structural size is shown in *Fig. 9*. In *Fig. 9*. (black line) all spatial coordinates are scaled by a factor *scale size*. Again it can be seen that a significant reduction of the energy barrier is obtained for *scale size* < 0.9 due to the annihilation of the skyrmions. For *scale size* > 1.0 the energy barrier slightly increases due to the overall larger magnetic volume, in particular thickness. In *Fig. 9* (red line) the thickness is kept constant to be *t* = 1,5 nm by rescaling the energy barrier assuming a linear dependence on the thickness. This is a reasonable assumption as discussed along the lines of *Fig. 8*. Here, it can be seen that there exists an optimal lateral dimension of the structure for *scale size* = 1 which corresponds to *l* = 500 nm, *w* = 75 nm, and *d* = 50nm which yields the highest energy barrier. However, this structure is already close to the smallest possible structure which allows for stable skyrmion motion. Hence, we will discuss in the following slightly larger structures which reliably lead to motion of the skyrmion over the pinning site.

In the following we calculate the spin torque efficiency for the structure of *l* = 600 nm, *w* = 90 nm, *t* = 1.8 nm which can be derived from the energy barrier and critical current

$$\eta = \Delta E / I_c = 0.19 \text{ } k_B T_{300} / \mu\text{A}.$$

Here, it might be important to note that the spin torque efficiency is basically independent on the film thickness, since both the energy barrier as well as the critical current depend linear on the film thickness in first order. The spin torque efficiency of a metallic MRAM junction simulated with the same spin diffusion approach is in similar order, $\eta = \Delta E / I_c = 0.16 \text{ } k_B T_{300} / \mu\text{A}$ [²³].

The spin torque efficiency for experimental CoFeB-MgO based tunnel junctions with diameters below 30 nm are in the range between 1 and 10 $k_B T/\mu A$ as reported in Ref [24]. Hence, the spin torque efficiency of skyrmion structures must be significantly improved to be in the order to reach spin torque efficiency of MRAM structures.

4. Discussion

In order to interpret the obtained storage densities of the presented skyrmion racetrack device we compare the obtained areal density of the skyrmion racetrack like device with the density of state of the art hard disk drives. For the smallest wire size (*size scale* = 0.9) where stable skyrmions are observed the width of the wire of $w = 75$ nm and the center to center distance between the pinning sites is 150nm. If we assume zero track distance between the wires this corresponds to an areal density of $A = 0.057$ Tbit/inch². For comparison the areal density of highest demonstrated heat assisted recording media is $AD = 1.402$ Tbit/inch² as reported in Ref[25]. The theoretical limit for heat assisted recording is in the range of $AD = 10$ Tbit/inch² Ref[26]. Even so the center to center distance between the pinning sites in the simulated skyrmion storage can be potentially reduced by a factor of 2-3, current hard disk densities with one layer of skyrmion storage devices are far out of reach and require breakthroughs such as multiple layers storing and moving skyrmion.

Another important topic for any skyrmion like device is the requirement for reliable depinning of the magnetic structure from the pinning cite. If current pulses are applied in the investigated skyrmion racetrack like structure the depinning process is a stochastic process due to finite temperature and will have further distribution in time due to imperfections of different pinning cites. The distribution of depinning time of field driven and current driven domain walls is investigated in various studies [27–30]. For MRAM structures in the dynamical switching regime the standard deviation of the switching time is in the order of 0.1 to 1 ns³¹.

In application the current pulse has to have a sufficient length and strength to get a high probability to move the topological structure over the first pinning cite. However, if the current pulse is too long one has high probability that one moves the topological structure too far over the second pinning site. Hence, the optimization of the correct pulse length is essential to avoid written in errors. Let us assume a structure where current pulse with a particular strength is applied which leads to 50% depinning probability at a pulse length t_a . Let us further assume that the derivative of the depinning probability is a Gaussian process with a standard deviation of the depinning time of σ . The probability that the structure depins within a time t_{pulse} is given by,

$$P_{\text{depinning}}(t_a, t_{\text{pulse}}, \sigma) = \int_0^{t_{\text{pulse}}} \frac{1}{\sigma\sqrt{2\pi}} \exp\left[-\frac{1}{2}\left(\frac{t-t_a}{\sigma}\right)^2\right] dt = -\frac{1}{2} \operatorname{erf}\left(\frac{t_a-t}{\sqrt{2}\sigma}\right) \Bigg|_0^{t_{\text{pulse}}} \quad (4)$$

If for example if $t_a = 1\text{ns}$ and $\sigma = 0.1\text{ns}$ the probability of depinning if a pulse length of $t_{\text{pulse}} = 2\text{ns}$ is applied is about 97.4 % which leads to significant write errors. The probability that depinning occurs can be increased if the current pulse length is increased, however than in turn there is an increased probability that the topological object moves too far over the next pinning sites. The probability that the structure moves over two pinning sites is the probability that at time t_1 in the interval dt_1 a

switching process occurs which is $\frac{\partial P_{\text{depinning}}(t_a, t_1, \sigma)}{\partial t_1} dt_1$ times the probability that in the remaining time $t_{\text{pulse}} - t_1$ the structure switches over the second pinning site. The total probability is given by,

$$\begin{aligned} P_{\text{depinning},2}(t_a, t_{\text{pulse}}, \sigma) &= \int_0^{t_{\text{pulse}}} P_{\text{depinning}}(t_a, t_{\text{pulse}} - t_1, \sigma) \frac{\partial P_{\text{depinning}}(t_a, t_1, \sigma)}{\partial t_1} dt_1 \\ &= P_{\text{depinning}}(2t_a, t_{\text{pulse}}, \sqrt{2}\sigma) \end{aligned} \quad (5)$$

The probability of a successful write process can be expressed as the probability that the structure moves across the first pinning site but does not move over the following pinning sites which is,

$$P_{\text{success}} = P_{\text{depinning}}(t_a, t_{\text{pulse}}, \sigma)(1 - P_{\text{depinning},2}(t_a, t_{\text{pulse}}, \sigma)) \quad (6)$$

Fig. 10 shows P_{success} as function of the pulse length t_{pulse} for $\sigma = 0.1\text{ ns}$ and $t_a = 1.0\text{ ns}$. It can be seen that for too short t_{pulse} the success rate is small since the topological structure cannot move over the first pinning site. For too long pulses the success rate is small again due to the high probability of write errors since the structure moves over the next pinning site. If the pulse length is $t_{\text{pulse}} = 3/2 \times t_a$ the highest success probability P_{success} is obtained. The success probability P_{success} is plotted as function of σ in *Fig. 10*. For a sigma of $\sigma = 0.1\text{ ns}$ and $\sigma = 0.01\text{ ns}$ the $P_{\text{success}} = 0.71$ and $P_{\text{success}} = 0.998$, respectively. Hence, a small standard deviation of the depinning time σ or a larger t_a is required. The time t_a can be increased by increasing the distance of adjacent bits or decreasing the speed of the topological object. Both possibilities lead to unwanted properties for data storage such as a sacrifices either data rate or data density. Hence, detailed optimizations and estimates are required in order discuss and overcome these challenges. A possibility to increases P_{success} might be to apply current pulses with different strength to use a small strength just to move the structure to the next pinning site. If the structure is definitely located next to the pinning site a high current pulse to overcome the pinning site can be applied. This clock cycle might lead to an increase of t_a but does not increase σ . The technological realization to overcome the before mentioned limits is regarded to by a very

challenging task requiring breakthroughs in the designs and concepts.

The financial support by the Austrian Federal Ministry of Science, Research and Economy and the National Foundation for Research, Technology and Development as well as the Austrian Science Fund (FWF) under Grant Nos. F4112 SFB ViCoM, I2214-N20 and the Vienna Science and Technology Fund (WWTF) under Grant No. MA14-044 is acknowledged.

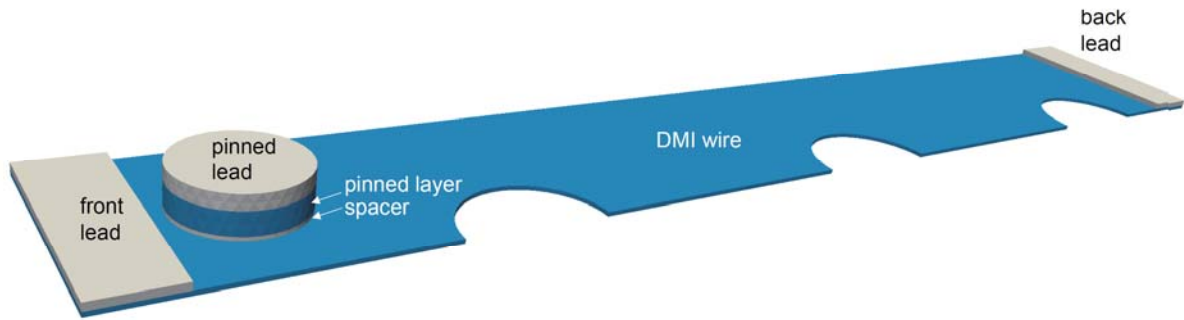


Fig. 1: Geometry of the used structure. The front and back lead has dimensions of 30 nm x 90 nm x 3nm. The dimensions of the DMI wire are $l = 600$ nm, $w = 90$ nm, $t = 1.8$ nm. The diameter of the notches as well of the spacer ($t = 1.5$ nm), pinned layer ($t = 9.0$ nm) and pinned lead ($t = 6.0$) is $d = 60$ nm.

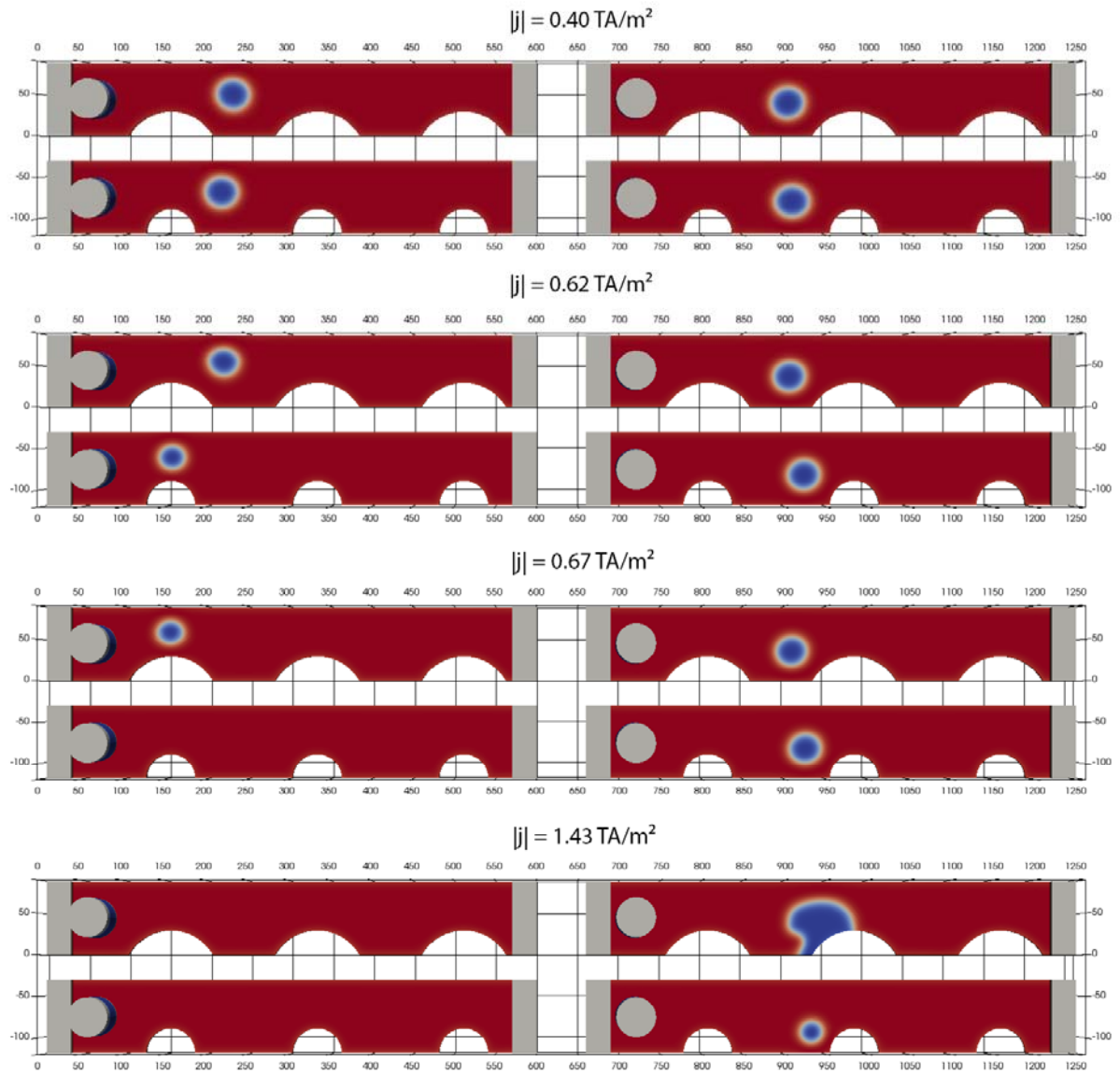


Fig. 2: Motion of the skyrmion as function of applied current density which is applied at the front lead. The dimensions of the wire are: $l = 600 \text{ nm}$, $w = 90 \text{ nm}$, $t = 1.8 \text{ nm}$. The diameter of the notches is $d = 60 \text{ nm}$ and $d = 120 \text{ nm}$, respectively. The given current density is the average density within the wire holding the skyrmion and the center between notches. (left column) a positive current density is applied at the right lead (right column) a negative current is applied at the right lead.

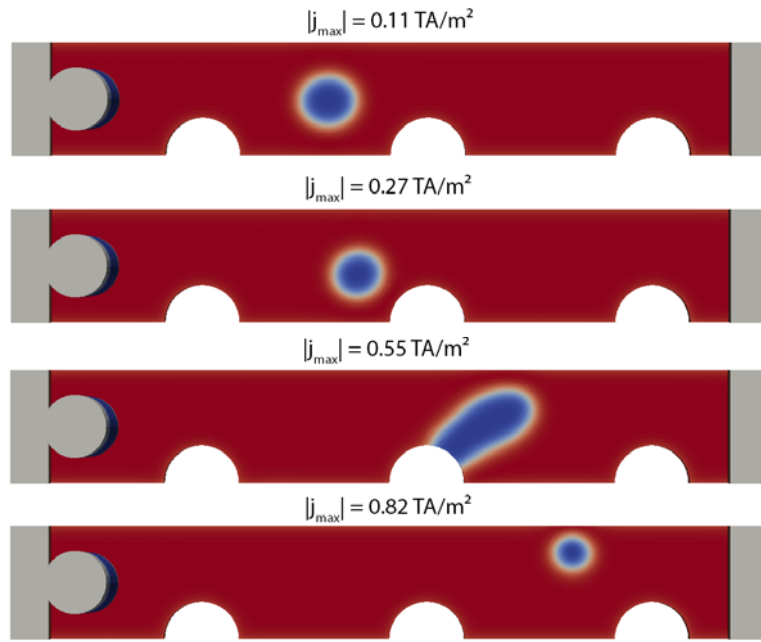


Fig. 3: Current pulses are applied from zero to j_{\max} within a time of 0.1 ns for the geometry of Fig. 2. After 0.1 ns the current is constant. The images show the transient states after 2 ns after the current is applied.

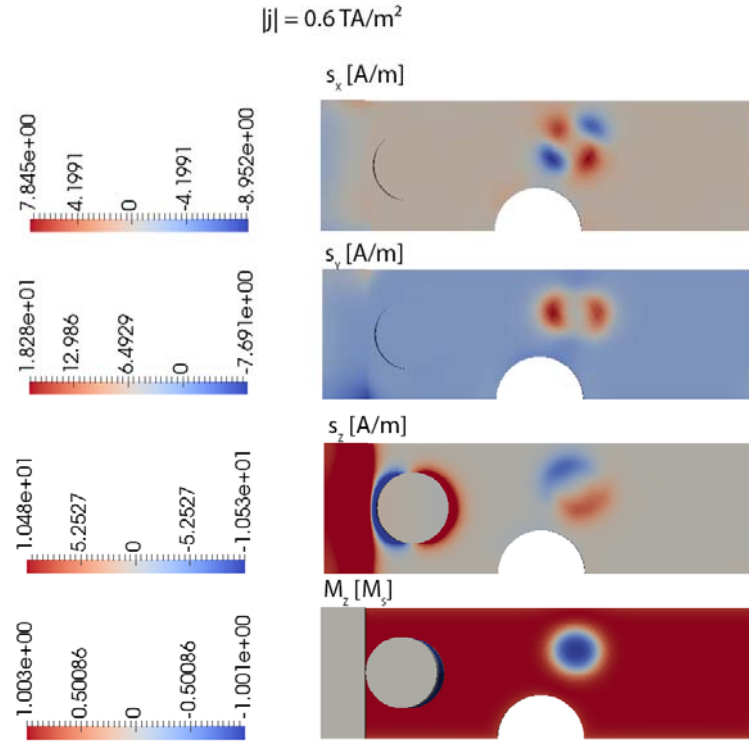


Fig. 4: x,y and z component of the spin-accumulation and magnetization before overcoming the pinning center. The lateral dimensions are as in Fig. 2. The diameter of the notches is $d = 60\text{nm}$.

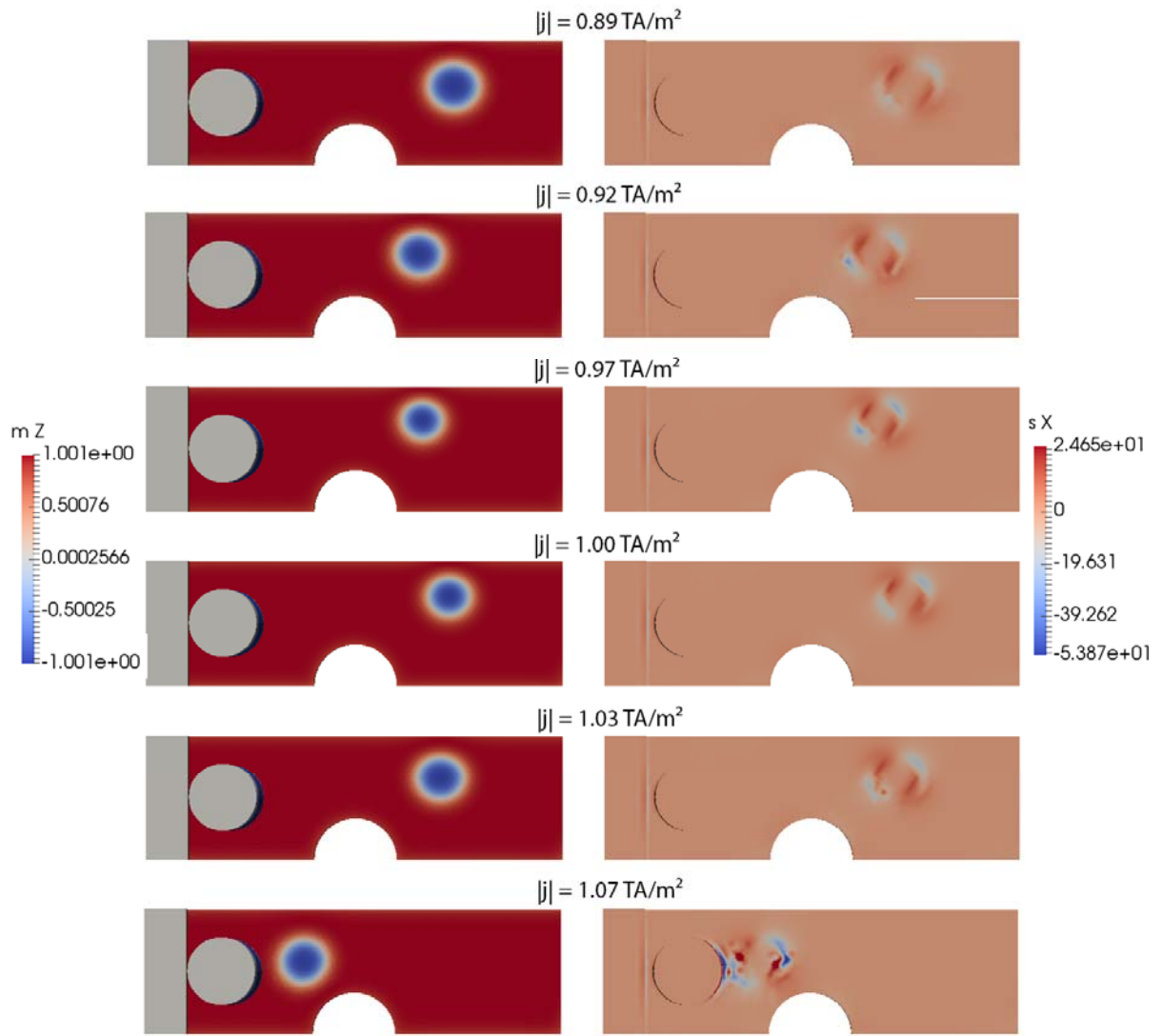


Fig. 5: Breathing modes of the simulation with $D_0 = 0$. Dimensions as according to Fig. 2. The y and z component of the spin accumulation are zero ($s_y = s_z = 0$) and are not shown.

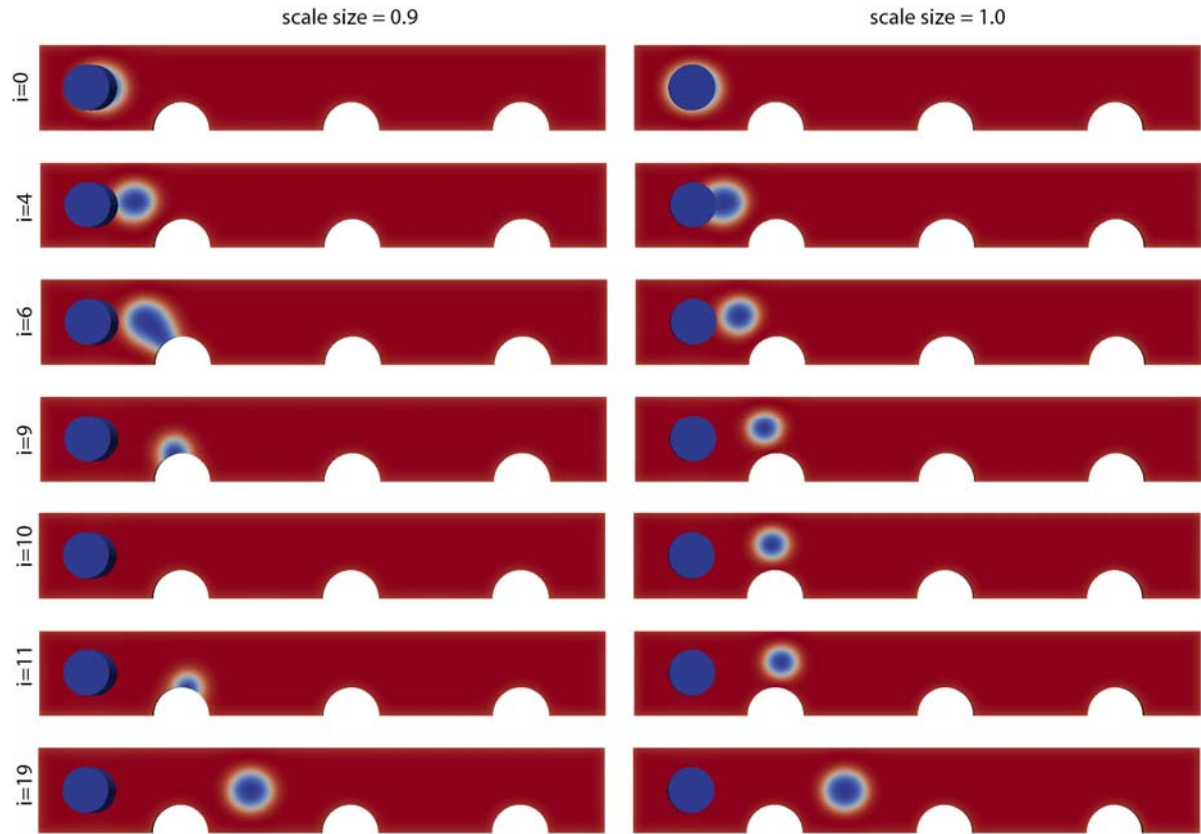


Fig. 6: States along the minimum energy path which is the most probable thermally activated reversal path. The saddle point configuration is for $i=10$. The minimum states are for $i=0$ and $i=19$ (right) the simulation correspond to the film of $l = 500$ nm, $w = 75$ nm, $t = 1.5$ nm and $d = 50$ nm. (left) all coordinates are scaled by a factor of 0.9.

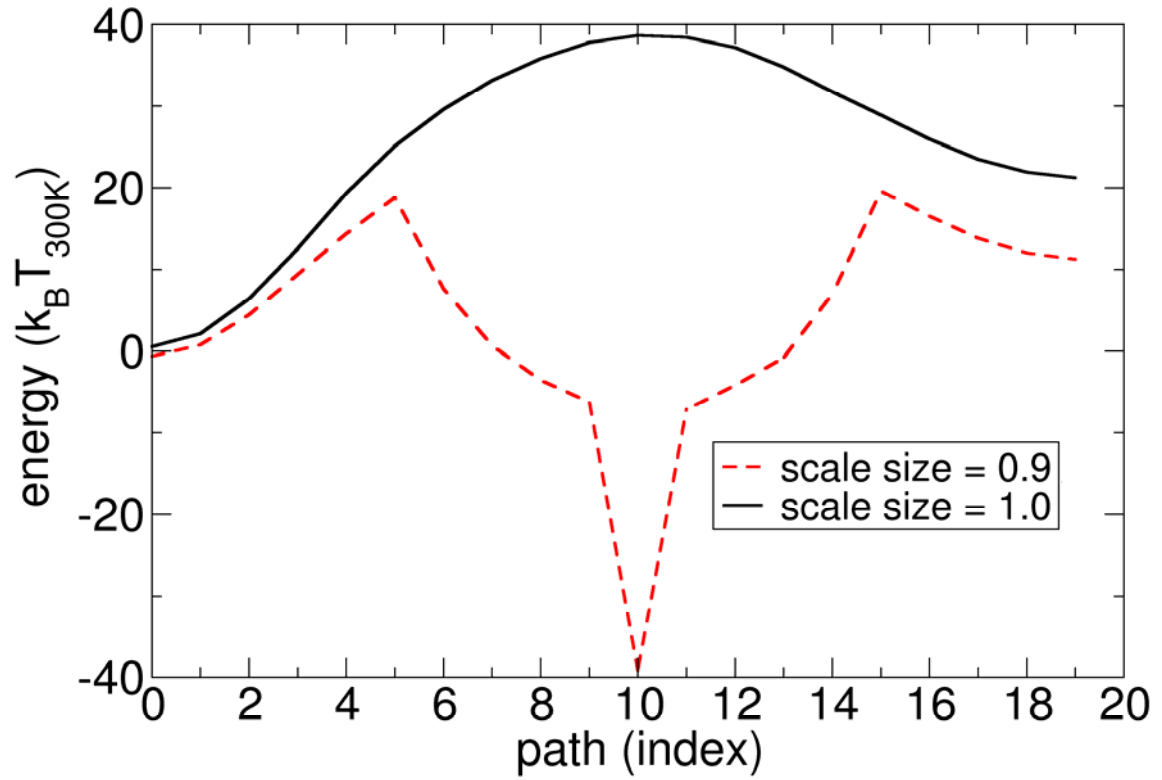


Fig. 7: Energy along the minimum energy path of the different states. The index i corresponds to the index i of Fig. 6. (black line) the simulation correspond to the film of $l = 500$ nm, $w = 75$ nm, $t = 1.5$ nm and $d = 50$ nm. (red dashed line) all coordinates are scaled by a factor of 0.9 .

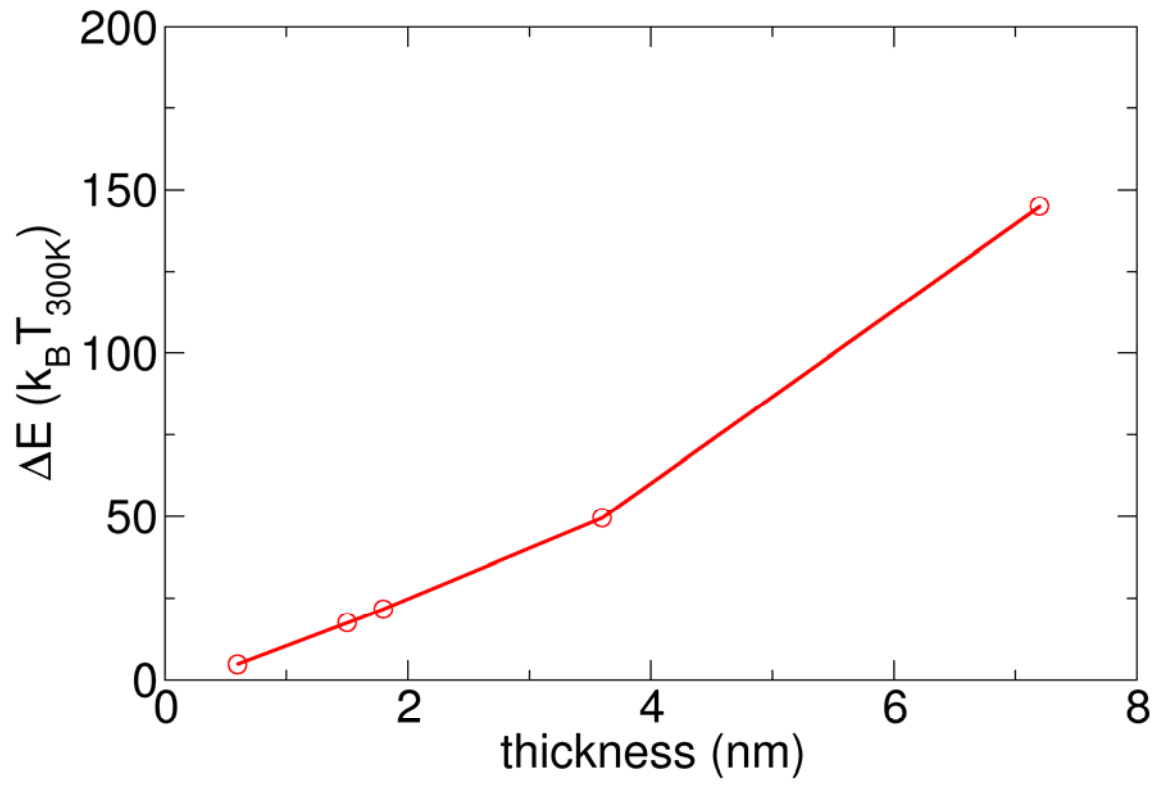


Fig. 8: Dependence of the energy barrier ΔE as function of the film thickness t . $l = 500$ nm, $w = 75$ nm, $d = 50$ nm.

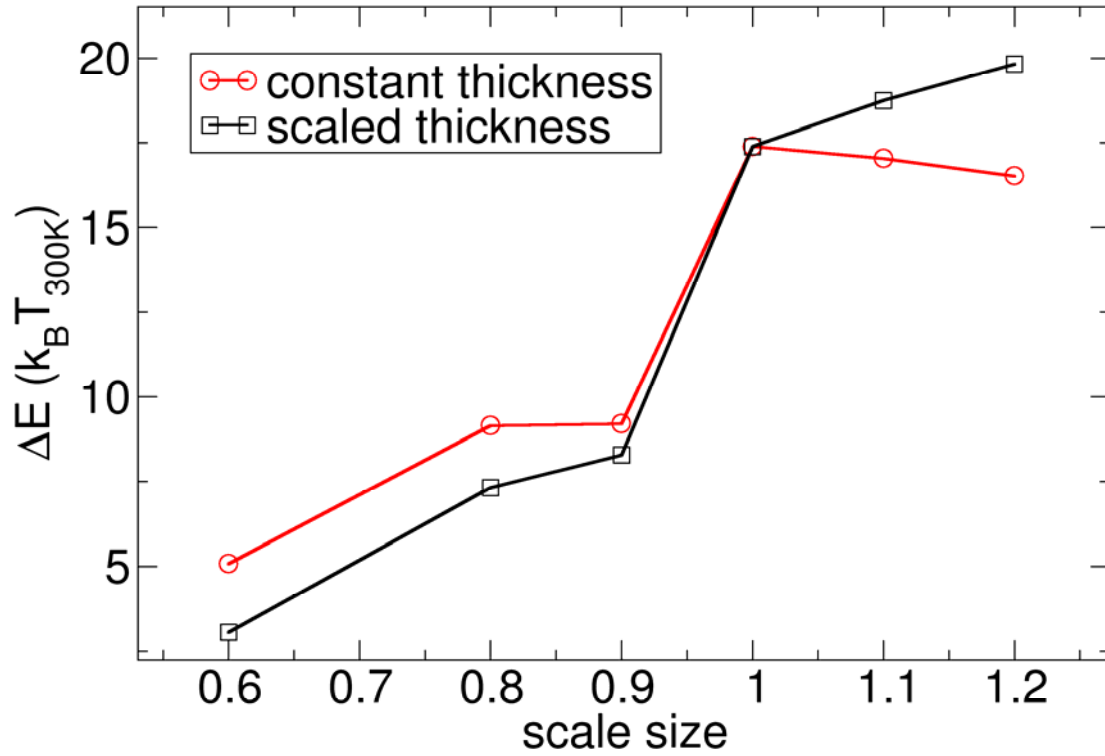


Fig. 9: Dependence of the energy barrier ΔE as function of the lateral dimension of the entire structure. The simulation with *scale size* = 1 corresponds to $l = 500$ nm, $w = 75$ nm, $t = 1,5$ nm and $d = 50$ nm (black line) all dimensions and structural features are scaled with the factor *scale size*. (red line) The thickness is kept constant to be $t = 1,5$ nm by rescaling the energy barrier assuming a linear dependence on the thickness. For all simulations with *scale* < 1 the skyrmion is annihilated at the notch.

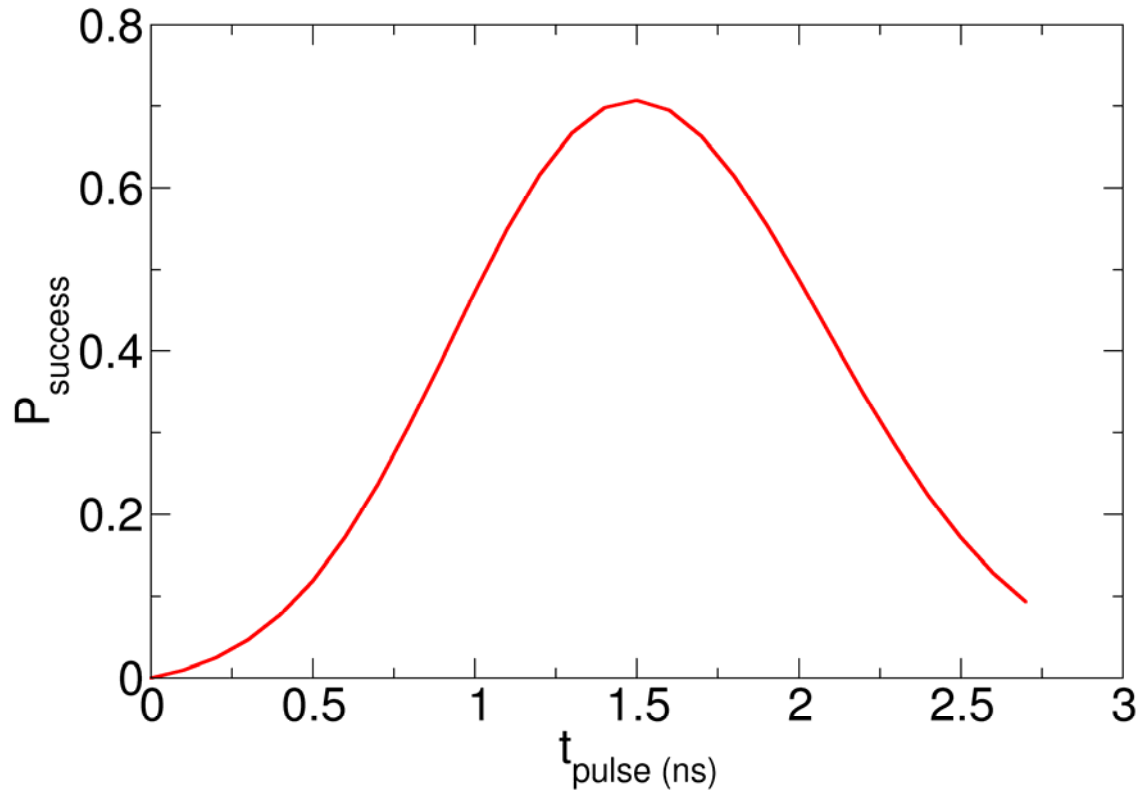


Fig. 10: Dependence of the probability for successful depinning (P_{success}) over one pinning site and not depinning over the second pinning site as a function of the length of the current pulse t_{pulse} . In this example $t_a = 1\text{ns}$ and $\sigma = 0.1\text{ ns}$.

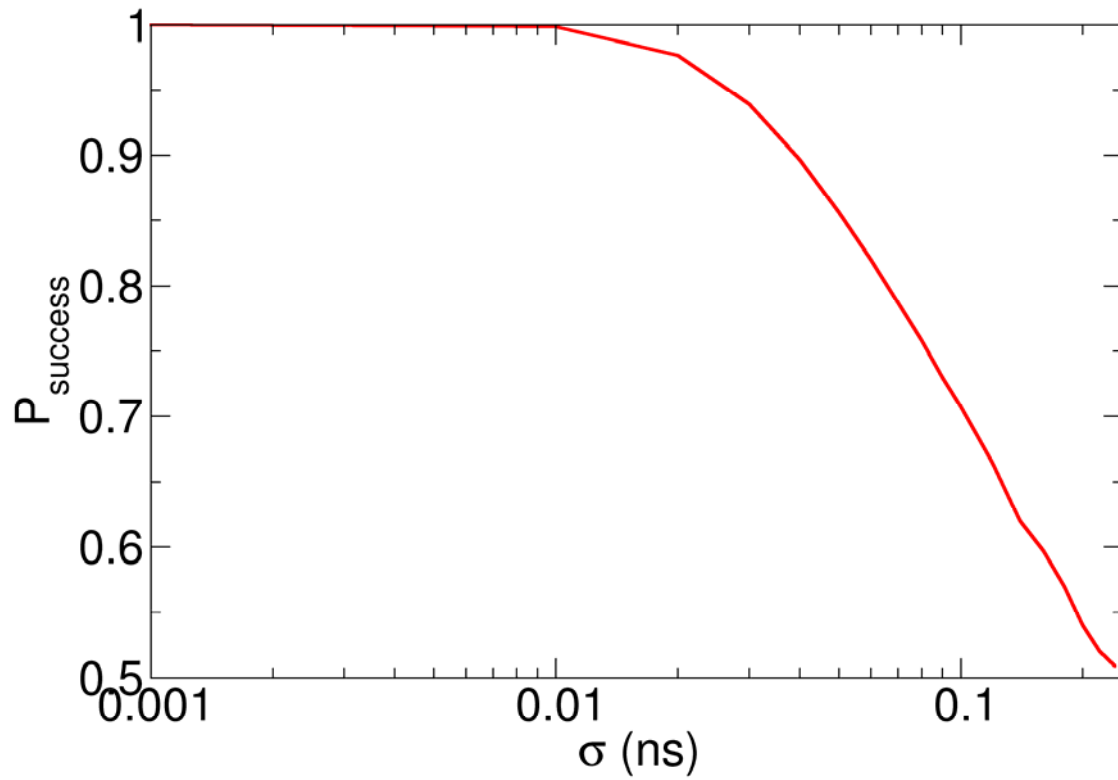


Fig. 11: Dependence of the probability for successful depinning over one pinning site and not depinning as function σ . For each σ the pulse length t_a was optimized to reach the highest P_{success} . $t_a = 1\text{ns}$.

1. Rößler, U. K., Bogdanov, A. N. & Pfleiderer, C. Spontaneous skyrmion ground states in magnetic metals. *Nature* **442**, 797–801 (2006).

2. Mühlbauer, S. *et al.* Skyrmion Lattice in a Chiral Magnet. *Science* **323**, 915–919 (2009).
3. Zhou, Y. & Ezawa, M. A reversible conversion between a skyrmion and a domain-wall pair in a junction geometry. *Nat. Commun.* **5**, 4652 (2014).
4. Yu, X. Z. *et al.* Skyrmion flow near room temperature in an ultralow current density. *Nat. Commun.* **3**, 988 (2012).
5. Jonietz, F. *et al.* Spin Transfer Torques in MnSi at Ultralow Current Densities. *Science* **330**, 1648–1651 (2010).
6. Tomasello, R. *et al.* A strategy for the design of skyrmion racetrack memories. *Sci. Rep.* **4**, 6784 (2014).
7. Wiesendanger, R. Nanoscale magnetic skyrmions in metallic films and multilayers: a new twist for spintronics. *Nat. Rev. Mater.* **1**, 16044 (2016).
8. Fert, A., Cros, V. & Sampaio, J. Skyrmions on the track. *Nat. Nanotechnol.* **8**, 152–156 (2013).
9. Zhang, S., Levy, P. M. & Fert, A. Mechanisms of Spin-Polarized Current-Driven Magnetization Switching. *Phys. Rev. Lett.* **88**, 236601 (2002).
10. Abert, C. *et al.* A three-dimensional spin-diffusion model for micromagnetics. *Sci. Rep.* **5**, (2015).
11. Suess, D., Fidler, J. & Schrefl, T. chapter 2 Micromagnetic Simulation of Magnetic Materials. *Handb. Magn. Mater.* **16**, 41–125 (2006).
12. Thiaville, A., Rohart, S., Jué, É., Cros, V. & Fert, A. Dynamics of Dzyaloshinskii domain walls in ultrathin magnetic films. *EPL Europhys. Lett.* **100**, 57002 (2012).
13. Djuhana, D., Supriyanto, E. & Kim, D. H. Micromagnetic Simulation of the Depinning Field Domain Wall on Symmetric Double Notch Ferromagnetic Wires. *Makara J. Sci.* 42–46 (2014).
doi:10.7454/mss.v18i2.3135
14. Lepadatu, S., Vanhaverbeke, A., Atkinson, D., Allenspach, R. & Marrows, C. H. Dependence of Domain-Wall Depinning Threshold Current on Pinning Profile. *Phys. Rev. Lett.* **102**, 127203 (2009).
15. Jiang, W. *et al.* Blowing magnetic skyrmion bubbles. *Science* **349**, 283–286 (2015).

16. Zhang, S., Levy, P. M. & Fert, A. Mechanisms of Spin-Polarized Current-Driven Magnetization Switching. *Phys. Rev. Lett.* **88**, 236601 (2002).
17. Thiaville, A., Nakatani, Y., Miltat, J. & Suzuki, Y. Micromagnetic understanding of current-driven domain wall motion in patterned nanowires. *EPL Europhys. Lett.* **69**, 990 (2005).
18. Zhou, Y. *et al.* Dynamically stabilized magnetic skyrmions. *Nat. Commun.* **6**, 8193 (2015).
19. Brown, W. F. Thermal Fluctuations of a Single-Domain Particle. *Phys. Rev.* **130**, 1677–1686 (1963).
20. Fiedler, G. *et al.* Direct calculation of the attempt frequency of magnetic structures using the finite element method. *J. Appl. Phys.* **111**, 093917 (2012).
21. E, W., Ren, W. & Vanden-Eijnden, E. String method for the study of rare events. *Phys. Rev. B* **66**, 052301 (2002).
22. APS -APS March Meeting 2016 - Event - Skyrmions in thin-film multilayers with interfacially-induced Dzyaloshinskii-Moriya interaction observed by MFM. in *Bulletin of the American Physical Society* **Volume 61, Number 2**, (American Physical Society).
23. Suess, D., Vogler, C., Bruckner, F., Sepehri-Amin, H. & Abert, C. Significant reduction of critical currents in MRAM designs using dual free layer with dynamical perpendicular and in-plane anisotropy. *ArXiv Prepr. ArXiv170200996* (2017).
24. Sun, J. Z. *et al.* Spin-torque switching efficiency in CoFeB-MgO based tunnel junctions. *Phys. Rev. B* **88**, 104426 (2013).
25. Ju, G. *et al.* High Density Heat-Assisted Magnetic Recording Media and Advanced Characterization #x2014;Progress and Challenges. *IEEE Trans. Magn.* **51**, 1–9 (2015).
26. Vogler, C., Abert, C., Bruckner, F., Suess, D. & Praetorius, D. Heat-assisted magnetic recording of bit-patterned media beyond 10 Tb/in². *Appl. Phys. Lett.* **108**, 102406 (2016).
27. Im, M.-Y., Bocklage, L., Fischer, P. & Meier, G. Direct Observation of Stochastic Domain-Wall Depinning in Magnetic Nanowires. *Phys. Rev. Lett.* **102**, 147204 (2009).

28. Burrowes, C. *et al.* Non-adiabatic spin-torques in narrow magnetic domain walls. *Nat. Phys.* **6**, 17–21 (2010).
29. Briones, J. *et al.* Stochastic and complex depinning dynamics of magnetic domain walls. *Phys. Rev. B* **83**, 060401 (2011).
30. Mihai, A. P. *et al.* Stochastic domain-wall depinning under current in FePt spin valves and single layers. *Phys. Rev. B* **84**, 014411 (2011).
31. Spin-transfer pulse switching: From the dynamic to the thermally activated regime. *Appl. Phys. Lett.* **97**, 262502 (2010).

